Vacuum-induced interference in light scattering by multilevel atomic chains

Aleksei Konovalov [1,2,*] Giovanna Morigi [2,3,†] and Nicola Piovella [4,‡]
[1]*Institute for Theoretical Physics, University of Innsbruck, A-6020 Innsbruck, Austria*
[2]*Theoretical Physics, Saarland University, D-66123 Saarbrücken, Germany*
[3]*Center for Quantum Technologies (QuTe), Saarland University, Campus, D-66123 Saarbrücken, Germany*
[4]*Dipartimento di Fisica "Aldo Pontremoli", Università degli Studi di Milano, Via Celoria 16, I-20133 Milano, Italy*

(Received 28 July 2026; accepted 27 October 2026; published 9 November 2026)

We investigate cooperative light scattering by an ordered chain of multilevel emitters, which possess two quasiresonant transitions with parallel dipole moments. Interference between dipole transitions induced by coupling with the vacuum gives rise to so called cross damping and cross shifts, that modify the incoherent and coherent dynamics and can be manifest in the spectroscopic properties of the emitted light. We determine the excitation spectrum when the emitters' chain is driven by an external laser in the limit in which the dipolar transitions can be described by harmonic oscillators and the scattering is coherent. We show that the interplay of multilevel interference and superradiance can give rise to measurable effects in chains of alkali-metal atoms.

DOI: 10.1103/fbdc-8n74

I. INTRODUCTION

Cooperative optical effects are one of the cornerstones of quantum optics [1]. When quantum emitters are at relatively high optical densities, they can behave as a collective entity whose optical properties differ from those of isolated atoms [1–3]. Superradiance [3,4], the enhanced cooperative light emission, is perhaps the most prominent example of such collective phenomena. A further prominent phenomenon is the dipole-dipole interactions mediated by multiple scattering processes [3,5–9].

In free space, these phenomena are especially pronounced when the interparticle distance is of the order of, or smaller than, the wavelength of the emitters' resonant transition [10–16]. Combining high-optical densities with spatially ordered structures, where the medium can form photonic band gaps [17–20], permits one to study the interplay between cooperative phenomena with the classical interference of the Bragg grating [21–24].

Experimental platforms such as optical lattices [25], arrays of optical tweezers [26–29], and ensembles of emitters in optical resonators [30–32] enable the realization of optically dense media with spatial periodicity of the order of the wavelength of the resonant light. The spatial long-range order in these systems provides unique conditions for observing quantum interference of scattered light [15,21,22,33–41]. In particular, when one of the lattice periods is a multiple of the transition wavelength, interference effects—and at high-optical density also dipole-dipole interactions—become especially pronounced [11–16]. This feature makes such systems promising platforms for exploring phenomena that require strong collective interactions [12,42–45].

Most theoretical analyses model the emitters with two-level transitions, often including Zeeman sublevels [37,38,46–48], while the role of the multilevel structures, including higher manifold, is relatively unexplored. This is typically justified since the atomic ensembles in most experiments are alkali metal, such that a closed two-level transition can be realized by optical pumping and sufficiently weak laser excitation. Nevertheless, even in this regime, high-precision spectroscopy experiments with single atoms reported features in the excitation spectrum due to off-resonant levels, arising from vacuum-induced interference effects [49–52]. Vacuum-induced interference refers to interference phenomena between electronic transitions coupled to common modes of the electromagnetic field [53,54]. Dipolar electronic transitions satisfying this condition are denoted by parallel dipoles. This interference also occurs when the electromagnetic field modes are in the vacuum [55–57], and is thus qualitatively different from interference phenomena of classical emitters. In what follows, we will refer to the terms describing this quantum interference as "cross-interference" and, when referring to dissipation, as "cross-damping" terms [49,58].

In this work, we analyze the scattering properties of a chain of multilevel emitters, setting our focus on the interplay between the multilevel interference and Bragg scattering. We analyze the problem in the regime of weak saturation, where scattering is prevailingly coherent and the emitters can be modeled by oscillators [46]. By means of an analytical model, we highlight the role of vacuum-induced interference in determining the scattering rates. We further analyze numerically the excitation spectra as a function of the chain periodicity for the parameters of the D2 line of ^{23}Na and of ^{7}Li atoms, in a regime consistent to the one of existing experimental platforms [59,60]. We finally discuss the robustness

*Contact author: aleksei.konovalov@uibk.ac.at
†Contact author: giovanna.morigi@physik.uni-saarland.de
‡Contact author: nicola.piovella@mi.infn.it

Published by the American Physical Society under the terms of the Creative Commons Attribution 4.0 International license. Further distribution of this work must maintain attribution to the author(s) and the published article's title, journal citation, and DOI.

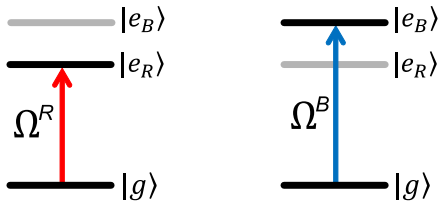


FIG. 1. Relevant level scheme of each emitter. The colored arrows denote only dipolar transitions which are involved in the excitation process, here labeled by the Rabi frequency multiplied by the corresponding Clebsch-Gordon coefficient. Both dipolar transitions are parallel and thus couple with the same modes of the electromagnetic field. Hence, spontaneous decay processes from the excited states can interfere. In this work, we assess the magnitude of this interference on coherent scattering when the emitters form a chain.

of vacuum-induced interference against atomic vibrations at the lattice sites, identifying the regime where the effects of vacuum-induced interference can be measurable.

This paper is organized as follows. In Sec. II, we introduce the model of coherent dipoles (MCD), formulated for a one-dimensional chain of multilevel quantum emitters. In Sec. III, we present an approximate analytic solution of the MCD for a general three-level system within a mean-field approach. Section IV is devoted to the excitation spectra of a transversely driven chain for the parameters of ^{23}Na or ^{7}Li atoms. The MCD is solved numerically and the results are compared with the analytic predictions of Sec. III. Finally, in Sec. V, we examine the robustness of cross-interference effects against atomic vibrations. The conclusions and outlooks are reported in Sec. VI. The Appendixes provide details of the model in Sec. II and of the analytical calculations in Secs. III and V.

II. THEORETICAL MODEL

We consider N identical emitters forming a regular, one-dimensional array. The emitters are localized at the positions $\vec{R}_\alpha = \alpha a\,\vec{e}_x$ (with $\alpha = 1, 2, \ldots, N$ and $\vec{e}_x$ the unit vector along x) and continuously driven by a monochromatic laser with electric field $\vec{E}_L$ and frequency ω_L. The relevant transitions of each emitter consist of a unique ground state and two excited states at frequency ω^i ($i = R, B$), where the two corresponding dipolar moments $\vec{d}^{\,i}$ are assumed to be parallel. The interactions of each emitter with light are treated in the electric-dipole approximation and the laser simultaneously drives both transitions with Rabi frequencies $\Omega^i = -\vec{d}^{\,i}\cdot\vec{E}_L/(2\hbar)$, as illustrated in Fig. 1. Moreover, photon emission by both transitions can interfere, giving rise to cross-damping and cross-interference dynamics. The interference takes place at the level of individual emitters and also between different emitters; the master equation has been derived in Ref. [61] and is reported in Appendix A.

In this work, we assume the weak-saturation regime, which allows us to set the ground-state population equal to unity and to approximate the dipolar transitions with harmonic oscillators, thus reducing the dynamics to a so-called model of coupled coherent dipoles [46–48,62]. In this limit, we denote by b^i_α the optical coherence of the dipolar transition i of the emitter at position $\vec{R}_\alpha$, while all other emitters are in the ground state. The equations of motion take the form

$$\dot{b}^i_\alpha = \sum_{j=R,B} b^j_\alpha\left(\mathrm{i}\Delta^{ij} - \frac{\Gamma^{ij}}{2}\right) - \mathrm{i}\Omega^i_\alpha - \sum_{\beta\neq\alpha,1}^{N}\sum_j G^{ij}_{\alpha\beta} b^j_\beta; \quad (1)$$

see Appendix A for details. Here, the first two terms on the right-hand side (rhs) are the single-emitter contributions, while the last term on the rhs accounts for collective effects. We first discuss the single-emitter part. Here, for $i = j$, $\Gamma^{ii} \equiv \Gamma^i$ is the linewidth of the dipolar transition i, $\Delta^{ii} \equiv \Delta^i_L = \omega_L - \omega^i$ is the laser detuning from the dipolar transition, and $\Omega^i_\alpha \equiv \Omega^i e^{\mathrm{i}\vec{k}_L\cdot\vec{R}_\alpha}$ is the Rabi frequency for the dipolar transition i, which depends on the position $\vec{R}_\alpha$ through the phase of the running wave $e^{\mathrm{i}\vec{k}_L\cdot\vec{R}_\alpha}$. The terms Γ^{RB}, Γ^{BR} and Δ^{RB}, Δ^{BR} give rise to cross damping and interference, respectively, induced by the coupling with vacuum and thermal fluctuations of the electromagnetic field modes [53,58]. Note that we have discarded the center-of-mass motion. Moreover, we assume optical transitions and neglect thermal effects since the mean photon number at optical frequencies and room temperature is negligible [61].

The last term on the rhs describes the interatomic coupling via the coherent and incoherent parts of the dipolar interaction through the Green's function,

$$G^{ij}_{\alpha\beta} = \frac{3\tilde{\gamma}^{ij}_{\alpha\beta}}{4}\frac{e^{\mathrm{i}kR_{\alpha\beta}}}{\mathrm{i}kR_{\alpha\beta}}\Big\{\left[\left(\vec{e}^{\,i*}_\alpha\cdot\vec{e}^{\,j}_\beta\right) - \left(\vec{e}^{\,i*}_\alpha\cdot\vec{e}_x\right)\left(\vec{e}^{\,j}_\beta\cdot\vec{e}_x\right)\right] + \left(\frac{1}{kR_{\alpha\beta}} - \frac{1}{\mathrm{i}(kR_{\alpha\beta})^2}\right)\left[\left(\vec{e}^{\,i*}_\alpha\cdot\vec{e}^{\,j}_\beta\right) - 3\left(\vec{e}^{\,i*}_\alpha\cdot\vec{e}_x\right)\left(\vec{e}^{\,j}_\beta\cdot\vec{e}_x\right)\right]\Big\}, \quad (2)$$

where $R_{\alpha\beta} = |\alpha - \beta|a$ is the linear distance between two emitters located at αa and βa, while $\vec{e}^{\,i}_\alpha = \vec{d}^{\,i}_\alpha/d^i_\alpha$ is the unit vector along the direction of the corresponding dipolar transition and $\vec{e}_x = \vec{R}_\alpha/|\vec{R}_\alpha|$. Note that since the dipolar transitions are parallel, $\vec{e}^{\,i*}_\alpha\cdot\vec{e}^{\,j}_\beta = 1$. The parameter scaling given by Eq. (2) has the dimension of a rate and reads

$$\tilde{\gamma}^{ij}_{\alpha\beta} = \frac{4}{3}\frac{d^{i*}_\alpha d^j_\beta}{\hbar c^3}\left(\frac{\omega^i + \omega^j}{2}\right)^3 \mathcal{F}^{ij}.$$

It describes the strength of dipolar transitions of different atoms, including the effect of identical transitions ($i = j$) as well as different transitions ($i \neq j$), and is scaled by the function $\mathcal{F}^{ij}$, which results from the systematic derivation of the coarse-grained master equation; see Appendix A. For the parameters considered in this work, $\mathcal{F}^{ij} \approx 1$. Thus, for $i = j$, $\tilde{\gamma}^{ii}_{\alpha\beta} = 4|d^i|^2(\omega^i/c)^3/3\hbar$ takes the form that is well known for two-level emitters [3]. For $i \neq j$, the rate $\tilde{\gamma}^{ij}_{\alpha\beta}$ depends on the average value between the two transition frequencies. We remark that the validity of the coherent-dipoles model in Eq. (1) is restricted to the weak-saturation regime, for $N\Omega^i \ll |\mathrm{i}\Delta^i_L - \Gamma^i/2|$.

In what follows, we will focus on chains composed of alkali-metal atoms. In this case, the assumption of a three-level transition, as we postulated in this section, is an oversimplification that, amongst others, artificially breaks the

spherical symmetry of each atom. In fact, this symmetry leads to vanishing cross-interference and cross-damping terms of the individual atoms, that is, $\Gamma^{i\neq j}=0$ and $\Delta^{i\neq j}=0$, when integrated over the full solid angle; see, e.g., Ref. [58]. On the other hand, multiple emitters ordered along a chain break the rotational symmetry of the array, leading to a finite contribution of the cross-interference and -damping terms between different atoms. In Ref. [61], we have performed a full numerical analysis of the interplay of single- and multi-emitter cross interference in the excitation spectra of two emitters. In the rest of this paper, we keep the three-level configuration, but set $\Gamma^{i\neq j}=0$ and $\Delta^{i\neq j}=0$ in Eq. (1). This permits us to single out the dependence of cross interference and damping on the spatial periodicity and determine their order of magnitude.

Our goal is to identify the contribution of cross interference in the photon-count signal (also known as the excitation spectrum) integrated over the full detection angle. In the low-saturation regime, it takes the form

$$S_\Omega(\delta_L)=\Gamma\sum_{\alpha=1}^{N}\sum_{i=R,B}\left|b_\alpha^i\right|^2+\sum_{\alpha=1}^{N}\sum_{\substack{\beta=1\\\beta\neq\alpha}}^{N}\sum_{i,j=R,B}2\mathrm{Re}\left(G_{\alpha\beta}^{ij}\right)b_\alpha^i b_\beta^{j*}, \tag{3}$$

where b_α^i is calculated in the steady state, after setting $\dot{b}_\alpha^i=0$ in Eq. (1).

III. MEAN-FIELD SOLUTION

We first consider the stationary solutions of Eqs. (1) in the mean-field limit, which we specify below. The mean-field treatment we consider here is valid in the limit of large chains when one can discard quantum correlations between the emitters and assume that the response is homogeneous. The first condition is warranted by the regime of sufficiently weak drives, where the internal emitters' transitions can be replaced by oscillators, and which is at the basis of the treatment of this paper. The second condition requires that the chain is homogeneously driven and that edge effects are negligible. In this treatment, the atomic density enters via the interparticle distance a and is a variable. This will provide insight into how cross interference between nondegenerate, yet parallel dipoles depends on a and influences resonance fluorescence.

1. Coherences

For simplicity, we assume $\Gamma_R=\Gamma_B=\Gamma$. We set $\dot{b}_i^\alpha=0$ and introduce the variable $\tilde{b}_\alpha^i=b_\alpha^i\exp(\mathrm{i}\vec{k}_L\cdot\vec{R}_\alpha)$, which satisfies the coupled equation

$$\tilde{b}_\alpha^i=\frac{\Omega^i}{\mathrm{i}\mathcal{D}^i}-\frac{1}{\mathcal{D}^i}\sum_{\beta(\neq\alpha)}^{N}\sum_{j=R,B}e^{-\mathrm{i}\vec{k}_L\cdot\vec{R}_{\alpha\beta}}G_{\alpha\beta}^{ij}\tilde{b}_\beta^j, \tag{4}$$

where $\mathcal{D}^i=\Gamma/2-\mathrm{i}\Delta^i$. We assume that each atom is equally affected by the entire ensemble and neglect edge effects, which is a valid approximation for sufficiently long arrays. In this regime, we denote the coherence $\tilde{b}_\alpha^i=b^i$, such that

$$b^i=\frac{\Omega^i}{\mathrm{i}\mathcal{D}^i}-\frac{1}{\mathcal{D}^i}\sum_{j=R,B}\langle G^{ij}\rangle b^j, \tag{5}$$

where the mean-field Green function reads

$$\langle G^{ij}\rangle=\frac{1}{N}\sum_{\alpha}^{N}\sum_{\beta(\neq\alpha)}^{N}e^{-\mathrm{i}\vec{k}_L\cdot\vec{R}_{\alpha\beta}}G_{\alpha\beta}^{ij}. \tag{6}$$

The formal solution of (5) takes the form

$$b^R=-\mathrm{i}\frac{\Omega^R(\mathcal{D}^B+\langle G^{BB}\rangle)-\langle G^{RB}\rangle\Omega^B}{(\mathcal{D}^R+\langle G^{RR}\rangle)(\mathcal{D}^B+\langle G^{BB}\rangle)-\langle G^{RB}\rangle\langle G^{BR}\rangle}, \tag{7a}$$

$$b^B=-\mathrm{i}\frac{\Omega^B(\mathcal{D}^R+\langle G^{RR}\rangle)-\langle G^{BR}\rangle\Omega^R}{(\mathcal{D}^B+\langle G^{BB}\rangle)(\mathcal{D}^R+\langle G^{RR}\rangle)-\langle G^{RB}\rangle\langle G^{BR}\rangle}, \tag{7b}$$

where each mean-field coherence contains variables associated with the other transition as well. If we formally set the cross-interference terms to zero, $\langle G^{RB}\rangle=0$ and $\langle G^{BR}\rangle=0$, then both coherences recover the known result for systems of emitters with no cross-interference terms between dipoles, $b^i=\frac{-\mathrm{i}\Omega^i}{\mathcal{D}^i+\langle G^{ii}\rangle}$ [46].

The solutions (7) are proper rational functions of the laser detuning and can be written as a sum of simple fractions, whose denominators determine the spectrum of the system. In further analysis of the solutions (7), we will see that the result depends on whether the driving laser is tuned close to either the lower- or higher-frequency transition. Hereafter, we refer to the transition, at which the laser is tuned close to resonance, as *driven*, while the other, which is distant by the frequency gap $\delta\omega$ (with $|\delta_L|\ll\delta\omega$), we call *interfering*.

We first investigate the case where the lower-frequency R transition is driven, that is, the laser frequency $\omega_L=\omega^R+\delta_L$ with $|\delta_L|\ll\delta\omega$. Similarly, the B transition is the interfering one, so that $\mathcal{D}^R=\Gamma/2-\mathrm{i}\delta_L$ and $\mathcal{D}^B=\Gamma/2+\mathrm{i}(\delta\omega-\delta_L)$, where $\delta\omega=\omega_B-\omega_R$. Then, up to the first-order correction in $\epsilon=\Gamma/\delta\omega\ll1$,

$$b^R_{\text{driven}}=b^{(0)R}+\epsilon b^{(1)R}, \tag{8a}$$

$$b^B_{\text{interfering}}=\epsilon b^{(1)B}, \tag{8b}$$

with the leading-order term

$$b^{(0)R}=-\mathrm{i}\frac{\Omega^R}{\Gamma^R/2-\mathrm{i}\delta_L} \tag{9}$$

describing the coherence for a collective excitation, with damping rate ($j=R,B$)

$$\Gamma^j=\Gamma+2\langle G^{jj}\rangle. \tag{10}$$

Hence, at lowest order, the emitters behave as two-level transitions. The terms in first order read

$$b^{(1)R}=\frac{\langle G^{RB}\rangle}{\Gamma^R/2-\mathrm{i}\delta_L}\left(\frac{\Omega^B}{\Gamma}-\frac{\Omega^R\langle G^{BR}\rangle}{\Gamma(\Gamma^R/2-\mathrm{i}\delta_L)}\right), \tag{11}$$

$$b^{(1)B}=-\frac{1}{\Gamma}\left(\Omega^B-\langle G^{BR}\rangle\frac{\Omega^R}{\Gamma^R/2-\mathrm{i}\delta_L}\right), \tag{12}$$

and include off-resonant excitation of single-atom transitions (first term on the rhs of $b^{(1)B}$) and multilevel interference (proportional to G^{RB} and/or G^{BR}).

Similarly, when the laser is tuned near the higher-frequency B transition, $\omega_L=\omega^B+\delta_L$, we obtain the solution by swapping the index $R\leftrightarrow B$ and the sign $\epsilon\to-\epsilon$ in Eqs. (8).

2. Cross-interference effects on the linewidth and frequency shift

Let us now discuss the spectral properties of the coherences (7); they can be extracted after inspecting the denominators. At first order in ϵ, the linewidth is given by

$$\langle \Gamma^R_{\rm CDR}\rangle = \Gamma + 2{\rm Re}\left(\langle G^{RR}\rangle + {\rm i}\frac{\langle G^{RB}\rangle\langle G^{BR}\rangle}{\delta\omega}\right), \tag{13}$$

and contains the superradiant contribution of two-level emitters known as the cooperative decay rate (CDR), as well as the cross-interference terms. The analogous expression for the lineshift reads

$$\langle \Lambda^R_{\rm CLS}\rangle = {\rm Im}\left(\langle G^{RR}\rangle + {\rm i}\frac{\langle G^{RB}\rangle\langle G^{BR}\rangle}{\delta\omega}\right), \tag{14}$$

where the first term is the linear contribution to the so-called collective Lamb shift (CLS) [47,48,59,63,64], while the second term is the contribution due to cross interference. Note that these cross-interference contributions have opposite influence on the lower- and higher-frequency transitions due to the sign inversion of the energy-gap parameter $\delta\omega$ in Eqs. (13) and (14).

3. Excitation spectrum

We now find an analytical form of the photon-count signal for the mean-field solution. From Eq. (3), we obtain

$$S(\delta_L) = \Gamma\sum_{i=B,R}|b^i|^2 + \sum_{i,j=B,R} 2{\rm Re}(\langle G^{ij}\rangle)\, b^i b^{j*}, \tag{15}$$

where b^i are given by Eqs. (7). Using Eq. (8), the excitation spectrum, up to the first order in ϵ, is the sum of two terms ($j = R$ or B),

$$S_j(\delta_L) = S^{(0)}_j(\delta_L) + \epsilon S^{(1)}_j(\delta_L), \tag{16}$$

where the zero-order term, for $j = R$,

$$S^{(0)}_R(\delta_L) = [\Gamma + 2{\rm Re}(\langle G^{RR}\rangle)]|b^{(0)R}|^2, \tag{17}$$

is the excitation spectrum in the absence of cross interference. Equation (17) has a Lorentzian shape centered on $\omega_R + {\rm Im}\{\Gamma_R\}$ with linewidth ${\rm Re}\{\Gamma_R\}$. The contribution of first order in ϵ modifies the Lorentzian profile and has the form

$$\begin{aligned} S^{(1)}_R(\delta_L) = {}& 2[\Gamma + 2{\rm Re}(\langle G^{RR}\rangle){\rm Re}(b^{(0)R}b^{(1)R*})] \\ & + 4{\rm Re}(\langle G^{RB}\rangle){\rm Re}(b^{(0)R}b^{(1)B*}). \end{aligned} \tag{18}$$

The excitation spectrum $S_B(\delta_L)$ close to the resonance at frequency ω_B is found analogously.

We remark that this analysis is valid at leading order in an expansion in $1/N$. Finite-size effects typically introduce corrections scaling with $1/N$. Some insight can be obtained for a fixed chain period $a = \lambda$. In this case, if one retains only the far-field terms, the mean-field Green function scales with N as $\ln(N)$.[1]

[1]If we take into account only the far-field terms $\sim\frac{1}{{\rm i}kR_{\alpha\beta}}$ in (2), then, in the case $a = 1\lambda$, the mean-field Green function reduces to a truncated harmonic series, $\langle G\rangle \sim \sum_{n=1}^{N}\frac{1}{n} - 1 \overset{N\gg 1}{=} \ln(N) + \gamma_E - 1$, where $\gamma_E \approx 0.5772$ is the Euler-Mascheroni constant. It is discussed in [16] for a case $N \to \infty$.

IV. EXCITATION SPECTRUM OF THE CHAIN

We now evaluate the excitation spectra for a periodic chain of atoms aligned along x and with period a. The atoms are continuously driven by a π-polarized laser whose polarization and wave vector are both oriented perpendicular to the chain axis. The configuration can be realized in existing experimental platforms [59,60]. The parameters we consider are the ones characterizing the two parallel transitions of the D2 line of (i) sodium ^{23}Na and (ii) lithium ^{7}Li, namely, the transitions between the ground state $S_{1/2}$ with $F = 2$, $M_F = 2$ and the excited states $P_{3/2}$ with quantum numbers $F' = 2$, $M_{F'} = 2$ and $F' = 3$, $M_{F'} = 2$, as detailed in Appendix B. We take two types of atoms to compare the influence of the cross-interference terms, which, as we can see from the results of the previous section, depend on the magnitude of the ratio, $\epsilon = \Gamma/\delta\omega$. We note that $\epsilon = 0.17$ for sodium [65], while $\epsilon = 0.65$ for lithium [66].

The spectrum, given by Eq. (3), is calculated by numerically solving the coupled equations (4) for various values of laser detuning. Figure 2 displays the result for a chain of 1000 emitters with the parameters of the sodium [Fig. 2(a)] and lithium [Fig. 2(b)] D2 line. Each signal consists of two peaks, shifted from the bare atomic transition frequencies. The result is compared with the mean-field result at zero and first order in ϵ. A net discrepancy between the numerical and perturbative results is visible in Fig. 2(b), where $\epsilon = 0.65$. This discrepancy can be completely attributed to the effect of the cross interference between multiple dipoles. In fact, as shown in the previous section, the smaller the energy gap between interfering dipoles, the stronger the impact of cross interference. Moreover, cross interference contributes to the R and B transitions in seemingly opposite ways, which is formally reflected by the sign reversal of the energy gap, $\delta\omega \to -\delta\omega$. Interestingly, the model which includes the cross-interference effects at first order in ϵ qualitatively reproduces the numerical results.

We now discuss the properties of the spectra as a function of the chain period. We numerically determine the spectrum on large chains for different values of a. We focus on the frequency shift and on the linewidth of the resonances with respect to the ones of the bare atom and we determine their value by fitting each spectrum close to the corresponding resonance. Based on the analytical results, given by Eq. (16), the numerical signals are fitted with Fano-like curves,

$$S_{\rm fit} = \sum_{i=R,B}\left(\frac{a_i}{\gamma_i^2/4 + (\Lambda_i - \delta_L)^2} + \delta_L\frac{b_i}{\gamma_i^2/4 + (\Lambda_i - \delta_L)^2}\right), \tag{19}$$

where the parameters $\{\gamma_i\}_{i=R,B}$ and $\{\Lambda_i\}_{i=R,B}$ correspond to the linewidths and line positions. Below we label the linewidth by CDR and the line shift by CLS.

Both analytic and numerical results are presented in Fig. 3 for the parameters of sodium and in Fig. 4 for the parameters of lithium and for periodicities $a > \lambda/2$. The behavior of the CDR as a function of the chain period resembles a

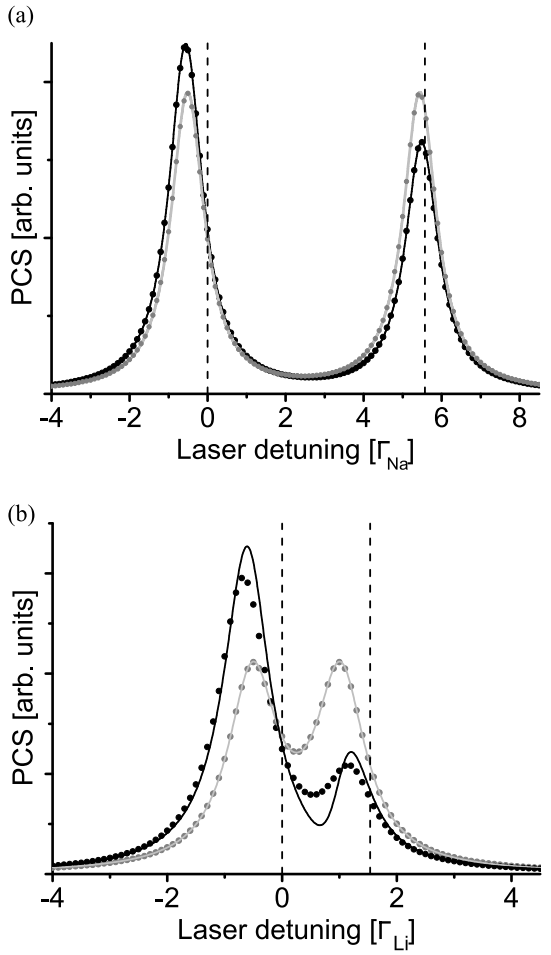


FIG. 2. The black dots are the photon-count signal, given by Eq. (3), vs laser detuning for a chain of $N = 1000$ emitters consisting of two parallel dipoles with the parameters of the (a) ^{23}Na and (b) ^{7}Li D2 line. The interparticle distance is $a = \lambda$, with λ the wavelength of the optical transition. Vertical dashed lines indicate the bare transition frequencies; the laser detuning is defined with respect to the lower-frequency transition. Solid lines correspond to the result in perturbation theory in ϵ; the gray solid line is found by setting all cross-interference terms to zero [$S_R^{(0)} + S_B^{(0)}$; see Eq. (17)]. The gray dots are the results of a simulation of the chain by artificially setting $G^{RB} = 0$ in Eq. (3). The black solid line includes the first-order corrections [$S_R + S_B$; see Eq. (16)] and qualitatively reproduces the numerical results summing up the individual contribution of the emitters along the chain.

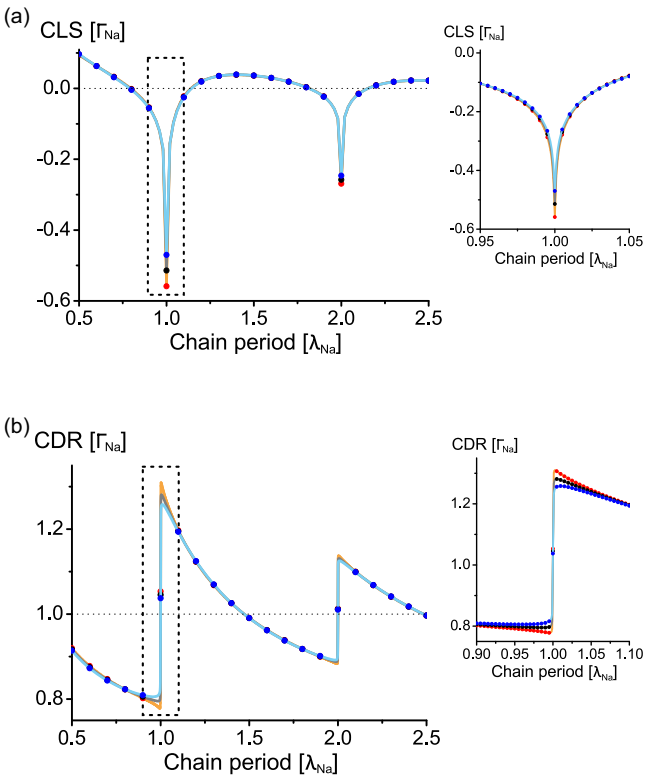


FIG. 3. Onset: (a) Line shift Λ_i (CLS) and (b) decay rate γ_i (CDR) as functions of the chain period and in units of Γ. The dots are the results of numerical integration of the excitation spectra for a chain of $N = 1000$ three-level emitters with the parameters of ^{23}Na and fitting using (19). The orange and cyan lines are the analytical results for the R and B transitions, respectively, as in Sec. III 2. For reference, the gray line shows the result when the cross-interference terms are set to zero in the model. It significantly overlaps with the predictions of the full model, except at periodicity $a \simeq \lambda, 2\lambda$. The insets display zooms into the region inside the corresponding box of the onset. Here, the predictions of the full model with cross interference are compared with the one of a model where cross-interference terms are set to zero (black). The red and blue dots refer to the R and B transitions, respectively.

sawtooth profile, while the corresponding dependence for the CLS is comblike. These results are consistent with those reported for chains of two-level emitters; see [12,16,67–69]. For chains with periods that are integer multiples of the transition wavelength, the effect of cross interference becomes visible. Moreover, significant differences appear between the predictions of the two- and three-level mean-field models, namely, the models without and with cross-interference terms. The discrepancy is especially pronounced in the depth of the CLS peaks. For lithium, the impact of cross interference is considerably stronger than for sodium, consistent with the photon-count signal results shown in Fig. 2. Notably, for chain period $a = \lambda$, the effect of cross interference on the CLS peak depth is comparable to that of the CLS itself. Figure 5 displays both linewidths and decay rates for periodicity in the subwavelength regime. The effects of cross interference become increasingly pronounced as a decreases. For periods $a \lesssim 0.15\lambda$, the influence of cross-interference terms leads to significant deviations from the prediction of a model, that discards these effects (gray line). These results highlight the necessity of including these effects in optically dense ensembles. In the following, we discuss the influence of residual atomic motion on the signal.

V. IMPACT OF ATOMIC MOTION

So far, we have assumed an idealized situation in which the atoms are fixed at given positions. We now include the effect of atomic motion by means of a phenomenological model in order to assess the impact on the excitation spectrum and, in particular, on the determination of the lineshift due to cross interference. We assume that the atoms are tightly bound at the

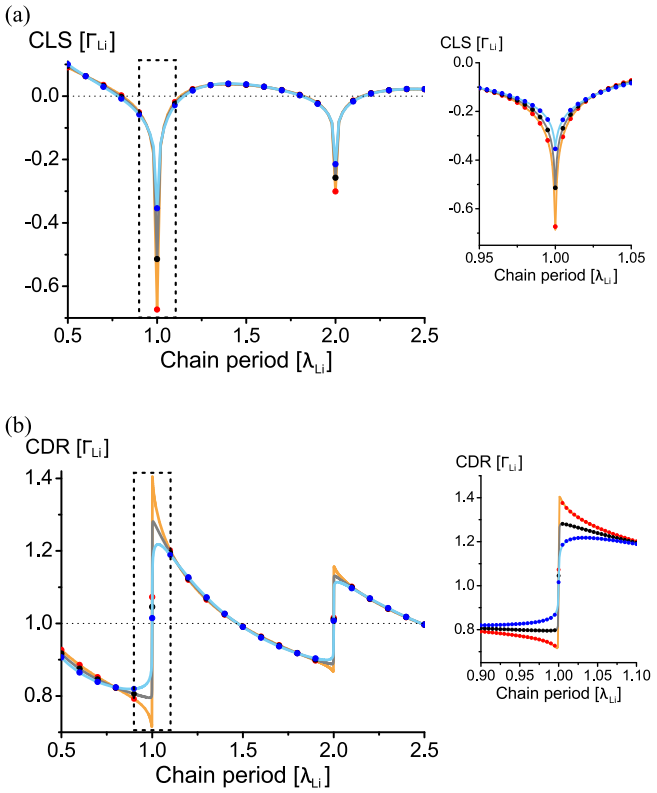


FIG. 4. Same as Fig. 3, but for the parameters of ^{7}Li.

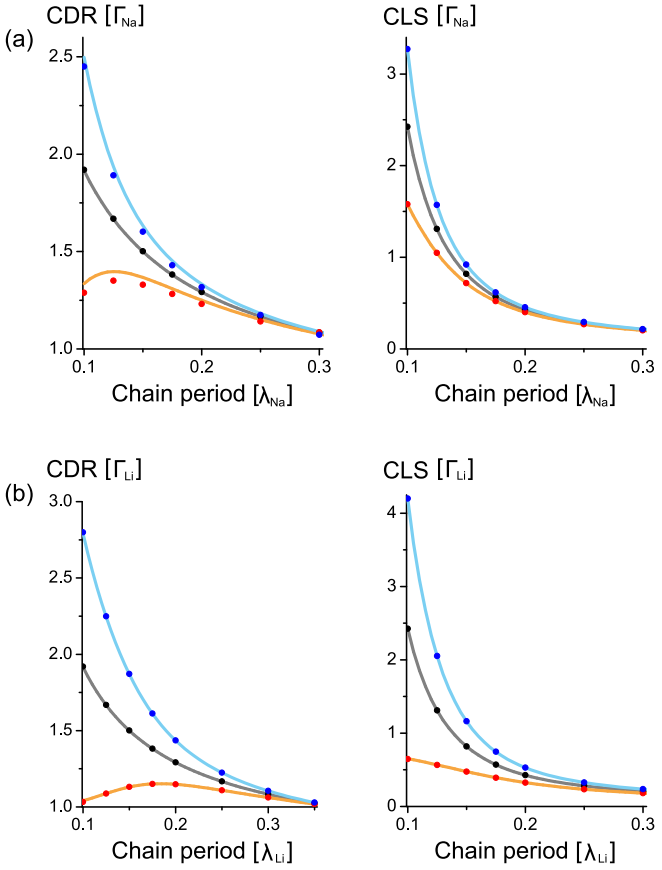


FIG. 5. CLR and CLS for the parameters of (a) sodium and (b) lithium and $a < \lambda/2$. The parameters and legenda are the same as in Figs. 3 and 4.

positions $\vec{R}_\alpha$ and perform uncorrelated fluctuations. We denote the displacement from $\vec{R}_\alpha$ by $\vec{r}_\alpha$. The density distribution of the atom at $\vec{R}_\alpha$ is then given by

$$n_\alpha(\vec{r}_\alpha) = \frac{1}{(\sqrt{\pi}\Delta)^3} e^{-\frac{(\vec{r}_\alpha)^2}{\Delta^2}}, \tag{20}$$

with Δ the width of the distribution, $\Delta \ll a, \lambda$. In this regime, $k\Delta \ll 1$. By performing a convolution of the Green function (2) at the positions of the atoms with their spatial distribution about $\vec{R}_\alpha$, we obtain

$$\bar{G}^{ij}_{\alpha\beta} \approx \left[1 - \tfrac{1}{2}(k\Delta)^2\right] G^{ij}_{\alpha\beta}(kR_{\alpha\beta}), \tag{21}$$

where we neglected terms $\sim \frac{(k\Delta)^2}{(kR)^3}, \frac{(k\Delta)^2}{(kR)^4}$ since they are of higher order. This result leads to a rescaling of the CDR and of the CLS by the factor $[1 - \frac{1}{2}(k\Delta)^2]$.

We compare this estimate with a numerical simulation, adding up the contributions of a chain, consisting of $N = 1000$ sodium atoms with a period $a = \lambda$, and determine the photon-count signal (3) by solving the MCD equations on the laser-detuning grid, $\delta_L \in \{-5\Gamma, \delta\omega + 4\Gamma\}$, here defined with respect to the eigenfrequency of the R transition of the bare atom. To assess the influence of the motion on the signal, we focus on the CLS. At fixed Δ, the spatial distribution (20) is simulated by solving the system of equations (4) numerically for N_c spatial configurations, according to the statistics of (20), and then averaging $S(\delta_L)$ over all configurations. The number of spatial configurations, N_c, is fixed in a such way that the mean-squared deviation of the CLS is less than $0.001\,\Gamma$: ranging from $N_c = 50$ for $\Delta = 0.01\lambda$ to $N_c = 500$ for $\Delta = 0.1\lambda$. The signals are fitted with the function (19) in order to extract the values of the lines' centers. The results are shown in Fig. 6.

In the limit of vanishing fluctuation amplitudes, $\frac{\Delta}{a} \to 0$, corresponding to the limit of the "pinned" atoms, the lineshifts are the ones shown in Fig. 3(b) at $a = \lambda$. As the width Δ of the spatial distribution increases, the absolute value of the lineshift decreases. The results of the numerical simulations agree reasonably well with the predictions from the lineshift rescaled by $[1 - \frac{1}{2}(k\Delta)^2]$ for widths $\Delta < 0.06\lambda$, while for $\Delta \gtrsim 0.07\lambda$, there is a growing mismatch. This behavior is expected, given that the Green function (21) is derived under the condition of small displacements. The convergence of the lineshifts towards the result obtained without cross interference clearly shows that motion tends to cancel the cross-interference effect. This trend highlights the increased sensitivity of cross interference to motional noise, which must be considered in the design and performance of potential experiments.

VI. CONCLUSIONS

We have analyzed the impact of vacuum-induced interference on the photon-count signal from a chain of emitters, composed of two parallel dipolar transitions, which are typically discarded when describing the superradiant scattering of optical dense media. In this paper, we have considered the

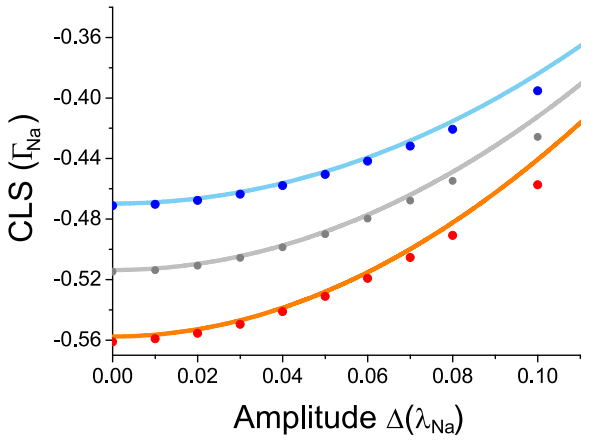


FIG. 6. The shift CLS for a chain with period $a = \lambda$ vs the position fluctuation amplitude Δ. The dots are obtained by numerically solving Eq. (3) for a chain of $N = 1000$ sodium atoms. The solid lines are the analytic predictions of the mean-field model, rescaled by the factor $[1 - (k\Delta)^2/2]$ (orange for R, cyan for B transition). The gray line is the prediction for a model where the cross-interference terms are set to zero. See text for details.

limit in which the dipolar transitions can be treated as coherent dipoles, and showed that the interplay of Bragg scattering and multilevel interference gives rise to visible effects, which lead to a qualitative modification of the excitation spectrum. This modification becomes enhanced the smaller the energy gap is between the two dipolar transitions and/or at subwavelength distances, and leads to qualitatively different shifts and linewidths of the resonances with respect to the predictions obtained when discarding vacuum-induced cross interference.

In this work, we took the parameters of the D2 line of alkali-metal atoms and demonstrated that cross interference shall be accounted for when describing scattering in optical dense media of multilevel emitters. We note that an accurate description of the spectroscopic signal shall include the full level structure of the D2 line, where the number of interfering channels is significantly larger than the reduced structure we considered. Moreover, the effects are expected to become more significant at saturation, where cross-damping terms become important.

ACKNOWLEDGMENTS

The authors wish to thank Tom Schmit for helpful comments. This work was partly performed in the framework of the European Training Network ColOpt, which was funded by the European Union (EU) Horizon 2020 programme under the Marie Sklodowska-Curie action, Grant Agreement No. 721465. G.M. acknowledges support from the German Research Foundation (DFG No. RTG-3082: Engineering covalent bonds in molecules and materials—Ec = m^2; Project No. 534930008).

DATA AVAILABILITY

There are no publicly available research data or software supporting this manuscript. Requests for further information or data should be sent to the authors.

APPENDIX A: COARSE-GRAINED MASTER EQUATION AND MODEL OF COHERENT DIPOLES

In this Appendix, we start from the coarse-grained master equation for multilevel emitters of Ref. [61] and systematically derive the model of coherent dipoles for the three-level emitter by performing a perturbative expansion in the saturation parameter.

1. Coarse-grained master equation

We report here the coarse-grained master equation of Ref. [61]. Let ρ be the density operator for the internal states of the emitters; then its dynamics is governed by the Born-Markov master equation,

$$\partial_t \hat{\rho} = \frac{1}{i\hbar}[\hat{H}_A + \hat{H}_S, \hat{\rho}(t)] + \mathcal{L}_D \hat{\rho}(t), \tag{A1}$$

where $\hat{H}_A$ is the Hamiltonian of the isolated emitters, including classical drives such as a laser, and in the absence of the coupling with the quantum electromagnetic field, while Hamiltonian $\hat{H}_S$ and superoperator (dissipator) $\mathcal{L}_D$ contain both the single-atom as well as the interatomic interference terms between parallel dipoles induced by the coupling with the quantum electromagnetic field.

Hamilton operator. The Hamiltonian term due to the interaction with the electromagnetic field (EMF) is given by the expression

$$\hat{H}_S = \sum_{\alpha} \langle \hat{V}_\alpha \rangle_R + \frac{1}{2} \sum_{\alpha,\beta} \hat{H}^S_{\alpha\beta},$$

where $\langle \hat{V}_\alpha \rangle_R$ is the expectation value of the interactions between field and emitters and here vanishes since we assume that the EMF is in the thermal state. The Hamilton operator $\hat{H}^S_{\alpha\beta}$ contains the frequency shifts and couplings due to the multilevel interference,

$$\hat{H}^S_{\alpha\beta} = -\hbar \sum_{i,j} \left[\left(\Delta^{\alpha\beta-}_{ij} + \Delta^{\alpha\beta(T)}_{ij} \right) \hat{\zeta}^{\alpha\dagger}_i \hat{\zeta}^{\beta}_j + \left(\Delta^{\alpha\beta+}_{ij} - \Delta^{\alpha\beta(T)}_{ij} \right)^* \hat{\zeta}^{\alpha}_i \hat{\zeta}^{\beta\dagger}_j \right] + \text{H.c.}, \tag{A2}$$

where $\hat{\zeta}^{\beta\dagger}_j \equiv |j_1\rangle_\beta \langle j_2|$ is the raising operator for the atom at position β exciting the dipolar transition j with state at lower energy j_2 and state at higher energy j_1 and dipole moment $\vec{D}^\beta_j$. The frequencies $\Delta^{\alpha\beta(T)}_{ij} = \Delta^{\alpha\beta-}_{ij}(T) - \Delta^{\alpha\beta+}_{ij}(T)$ and the

individual coefficients read (below in Gauss units)

$$\Delta_{ij}^{\alpha\beta\pm} = \Theta_{ij}^{(\Delta t)} \frac{\vec{D}_i^{\alpha*}\cdot\vec{D}_j^{\beta}}{(2\pi)^2\hbar c^3}\mathcal{P}\int_0^{\omega_{\rm cut}} \frac{d\omega\,\omega^3}{\omega\pm\omega_{ij}} F_{\alpha\beta}^{ij}(\vec{R}_{\alpha\beta}), \tag{A3}$$

$$\Delta_{ij}^{\alpha\beta\pm}(T) = \Theta_{ij}^{(\Delta t)} \frac{\vec{D}_i^{\alpha*}\cdot\vec{D}_j^{\beta}}{(2\pi)^2\hbar c^3} \times \mathcal{P}\int_0^{\omega_{\rm cut}} \frac{d\omega\,\omega^3 n(\omega,T)}{\omega\pm\omega_{ij}} F_{\alpha\beta}^{ij}(\vec{R}_{\alpha\beta}). \tag{A4}$$

Here, $\mathcal{P}$ denotes the Cauchy principal value and $\omega_{\rm cut}$ is the cutoff frequency. The frequency

$$\omega_{ij} = \frac{\bar{\omega}_i + \bar{\omega}_j}{2}$$

is the average between the two transition frequencies, and the coefficient $F_{\alpha\beta}^{ij}(\vec{R}_{\alpha\beta})$ also depends on the distance $\vec{R}_{\alpha\beta} = \vec{R}_\alpha - \vec{R}_\beta$ between the atoms and on the wave number $k = \omega/c$. It takes the form

$$F_{\alpha\beta}^{ij}(\vec{R}_{\alpha\beta}) = 4\pi\left(j_0(kR_{\alpha\beta})\left[1 - \frac{\left(\vec{D}_i^{\alpha}\cdot\vec{R}_{\alpha\beta}\right)^*\left(\vec{D}_j^{\beta}\cdot\vec{R}_{\alpha\beta}\right)}{D_i^{\alpha}D_j^{\beta}R_{\alpha\beta}^2}\right] - \frac{j_1(kR_{\alpha\beta})}{kR_{\alpha\beta}}\left[1 - \frac{3\left(\vec{D}_i^{\alpha}\cdot\vec{R}_{\alpha\beta}\right)^*\left(\vec{D}_j^{\beta}\cdot\vec{R}_{\alpha\beta}\right)}{D_i^{\alpha}D_j^{\beta}R_{\alpha\beta}^2}\right]\right), \tag{A5}$$

where we used the notation $D_i^\alpha = |\vec{D}_i^\alpha|$ and $R_{\alpha\beta} = |R_{\alpha\beta}|$. Here, $j_0(x)$ and $j_1(x)$ are spherical Bessel functions of the first type. The dependence on the vector joining the atoms breaks the spherical symmetry and is at the origin of the anisotropic light emission of superradiance.

Dissipator. The Lindblad term $\mathcal{L}_D$ describes the incoherent processes. It can be decomposed into the sum

$$\mathcal{L}^D\hat{\rho}(t) = \sum_{\alpha,\beta}\mathcal{L}_D^{\alpha\beta}\hat{\rho}(t), \tag{A6}$$

where the terms with $\alpha = \beta$ describe the dissipation of N noninteracting atoms, while the terms with $\alpha \neq \beta$ originate from multiple scattering of resonant photons and vanish when the distance between the atoms exceeds several wavelengths. The individual terms read

$$\mathcal{L}_D^{\alpha\beta}\hat{\rho}(t) = \sum_{i,j}[1+n(\omega_{ij},T)] \times\left\{\frac{\Gamma_{\alpha\beta}^{ij}}{2}\left[\hat{\zeta}_j^{\beta}\hat{\rho}(t),\hat{\zeta}_i^{\alpha\dagger}\right] + \frac{\Gamma_{\alpha\beta}^{ij}}{2}\left[\hat{\zeta}_j^{\beta},\hat{\rho}(t)\hat{\zeta}_i^{\alpha\dagger}\right]\right\} + \sum_{i,j} n(\omega_{ij},T) \times\left\{\frac{\Gamma_{\alpha\beta}^{ij*}}{2}\left[\hat{\zeta}_j^{\beta\dagger}\hat{\rho}(t),\hat{\zeta}_i^{\alpha}\right] + \frac{\Gamma_{\alpha\beta}^{ij*}}{2}\left[\hat{\zeta}_j^{\beta\dagger},\hat{\rho}(t)\hat{\zeta}_i^{\alpha}\right]\right\}, \tag{A7}$$

where $n(\omega,T) = 1/(e^{\beta\hbar\omega}-1)$ is the mean photon number at temperature $T = 1/k_B\beta$. The damping coefficients take the form

$$\Gamma_{\alpha\beta}^{ij} = \Theta_{ij}^{(\Delta t)}\frac{\vec{D}_i^{\alpha*}\cdot\vec{D}_j^{\beta}}{2\pi\hbar c^3}\omega_{ij}^3 F_{\alpha\beta}^{ij}(k_{ij}), \tag{A8}$$

with $k_{ij} = \frac{\omega_{ij}}{c}$. We note that for $i \neq j$, the damping coefficients are different from zero if the scalar product $\vec{D}_i^{\alpha*}\cdot\vec{D}_j^{\beta} \neq 0$. Finally,

$$\Theta_{ij}^{(\Delta t)} = \frac{\sin[(\omega_i+\omega_j)\Delta t/2]}{(\omega_i+\omega_j)\Delta t/2}, \tag{A9}$$

and results from the procedure of coarse graining. This term selects transitions which are resonant within the resolution set by the coarse-graining time Δt. For optical transitions, this factor selects a pair of frequencies ω_i and ω_j with opposite signs. Correspondingly, it selects terms in the Hamiltonian and dissipator where the pairs of operators $\hat{\zeta}_i^{\alpha\dagger}\hat{\zeta}_j^{\beta}$ describe an excitation and a deexcitation along two (quasi)resonant transitions. See [58,61].

2. Derivation of the model for coupled coherent dipoles

We now consider a chain composed of N identical emitters uniformly driven by the laser. We now assume that the internal levels of the emitter consist of the ground state $|g\rangle$ and excited states $|R\rangle$ and $|B\rangle$, with parallel dipolar moments $\vec{d}^R \equiv \vec{D}_i$ with $i = (g,R)$ and $\vec{d}^B \equiv \vec{D}_j$ with $j = (g,B)$. Hamiltonian $\hat{H}_A = \sum_\alpha \hat{H}_A^\alpha$ is the sum of the Hamiltonian for each emitter,

$$\hat{H}_A^\alpha = -\sum_{R,B}\hbar\Delta^i|i\rangle_\alpha\langle i| + \hbar\left(\Omega_\alpha^i|i\rangle\langle g| + \text{H.c.}\right), \tag{A10}$$

and is reported in the reference frame rotating at the laser frequency ω_L. Here, $\Omega_\alpha^i = \Omega^i e^{i\vec{k}_L\cdot\vec{R}_\alpha}$. In what follows, we assume optical transitions and discard thermal effects because the mean photon number at optical frequencies and room temperature is negligible. Therefore, we set $n(\omega_{ij},T) = 0$ and, consequently, discard the contribution of thermal shifts $\Delta_{ij}^{\alpha\beta\pm}(T)$ to the Hamiltonian $\hat{H}_S$, as well as the thermal contributions to the dissipator.

The weak-saturation regime is defined by the small parameter $\mathcal{S} = N\Omega/|\Delta^i - i\Gamma/2| \ll 1$. The state $|G\rangle = \otimes_{\alpha=1}^N|g\rangle_\alpha$ is the ground state of the chain and has occupation $\rho_{GG} \equiv \langle G|\hat{\rho}|G\rangle \sim 1$. The optical coherences between $|G\rangle$ and the excited state $|e_\alpha^i\rangle \equiv |g_1,\ldots,e_\alpha^i,\ldots,g_N\rangle$ are $\langle e_\alpha^i|\hat{\rho}|G\rangle \sim \mathcal{S}$, while all other terms are of higher order and are neglected here. Following this procedure, the matrix elements $b_\alpha^i = \langle e_\alpha^i|\hat{\rho}|G\rangle$ (optical coherences) of master equation (A1) take the form

$$\dot{b}_\alpha^i = -i\left(\omega^i - \omega_L - i\frac{\Gamma_\alpha^i}{2}\right)b_\alpha^i - i\Omega_\alpha^i\rho_{G,G} - \sum_{\beta,\alpha=1}^N\sum_j G_{\alpha\beta}^{ij}b_\beta^j, \tag{A11a}$$

and then replace $\rho_{GG} = 1$ at first order in $\mathcal{S}$; we refer the reader to Refs. [48,70] for analogous treatments where the ground state is not unique. The definitions of the individual terms are reported in Sec. II; however, note that the sum over the emitters here contains the cross-damping and interference terms of the individual emitter as it contains the term $\alpha = \beta$. The term $\mathcal{F}^{ij}(\Delta t)$ approximates the function $\Theta_{ij}^{(\Delta t)}$ using the

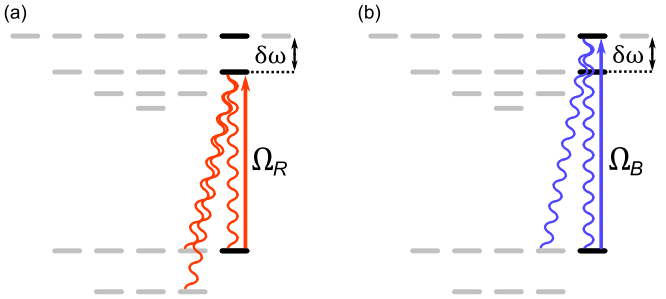


FIG. 7. Level structure for the D2 line of ^{23}Na atom. In the atom, initially prepared in the polarized ground state $|g^{F=2,M_F=2}\rangle$ and illuminated by a π-polarized laser, two transitions can occur: (a) lower frequency $|3S_{\frac{1}{2}}, F=2, M_F=2\rangle \to |3P_{\frac{3}{2}}, F'=2, M_{F'}=2\rangle$ and (b) higher frequency $|3S_{\frac{1}{2}}, F=2, M_F=2\rangle \to |3P_{\frac{3}{2}}, F'=3, M_{F'}=2\rangle$, referred to as R and B in the main text. The excitations undergo the subsequent decay processes denoted with wiggling lines. In our study, we ignore the decay channels to states with $M_F < 2$.

convolution with a Gaussian [58,61],

$$\mathcal{F}^{ij}(\Delta t) = \frac{2}{\sqrt{\pi}\tau}\int_0^\infty \frac{\sin\left[\frac{\tau}{2}(\omega^i-\omega^j)\right]}{\frac{\tau}{2}(\omega^i-\omega^j)} e^{-\frac{\tau^2}{\Delta t^2}} d\tau. \quad \text{(A12)}$$

Here, Δt is a coarse-graining time, a timescale in the range $\tau_R \ll \Delta t \ll \tau_A$, between τ_R and the characteristic timescale τ_A of the system's internal dynamics. For degenerate dipoles, this coefficient is unity. For the case $|\omega^i - \omega^j|^{-1} \gg \tau_R$, which is considered in the present work, $\mathcal{F}^{ij}(\Delta t) \approx 1$.

APPENDIX B: LEVEL STRUCTURE OF LINE D2 OF ALKALI ATOMS ^{7}Li AND ^{23}Na

In this Appendix, we provide details and parameter values for the D2 transition line, which are relevant to the calculations presented in the main text. Both isotopes, ^{7}Li and ^{23}Na, have a single optical electron in the outer shell and a nuclear spin $I = \frac{3}{2}$. The relevant level structures are shown in Figs. 7 and 8 for the ^{23}Na and ^{7}Li atoms, respectively. For the ^{23}Na atom, the relevant dipolar transitions are

$$R : \left|3S_{\frac{1}{2}}^{F=2,M_F=2}\right\rangle \to \left|3P_{\frac{3}{2}}^{F'=2,M_{F'}=2}\right\rangle,$$
$$B : \left|3S_{\frac{1}{2}}^{F=2,M_F=2}\right\rangle \to \left|3P_{\frac{3}{2}}^{F'=3,M_{F'}=2}\right\rangle.$$

The energy gap between the nondegenerate dipoles is taken $\frac{\delta\omega}{2\pi} = 58.326$ MHz and the decay rate is $\frac{\Gamma}{2\pi} = 9.795$ MHz [65].

For the atom ^{7}Li, the relevant dipolar transitions are

$$R : \left|2S_{\frac{1}{2}}^{F=2,M_F=2}\right\rangle \to \left|2P_{\frac{3}{2}}^{F'=3,M_{F'}=2}\right\rangle,$$
$$B : \left|2S_{\frac{1}{2}}^{F=2,M_F=2}\right\rangle \to \left|2P_{\frac{3}{2}}^{F'=2,M_{F'}=2}\right\rangle.$$

The energy gap between the nondegenerate dipoles is taken $\frac{\delta\omega}{2\pi} = 9.2$ MHz and the decay rate is $\frac{\Gamma}{2\pi} = 6$ MHz [66].

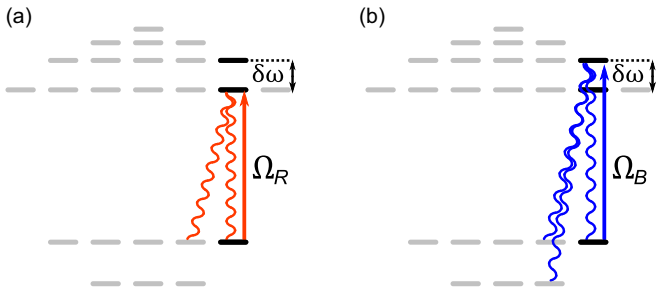


FIG. 8. Same as Fig. 7, but for the level structure for the D2 line of the ^{7}Li atom.

[1] M. Reitz, C. Sommer, and C. Genes, Cooperative quantum phenomena in light-matter platforms, PRX Quantum **3**, 010201 (2022).

[2] K. Hepp and E. H. Lieb, On the superradiant phase transition for molecules in a quantized radiation field: The Dicke maser model, Ann. Phys. **76**, 360 (1973).

[3] M. Gross and S. Haroche, Superradiance: An essay on the theory of collective spontaneous emission, Phys. Rep. **93**, 301 (1982).

[4] R. H. Dicke, Coherence in spontaneous radiation processes, Phys. Rev. **93**, 99 (1954).

[5] D. O'Dell, S. Giovanazzi, G. Kurizki, and V. M. Akulin, Bose-einstein condensates with $1/r$ interatomic attraction: Electromagnetically induced "gravity", Phys. Rev. Lett. **84**, 5687 (2000).

[6] H. Ritsch, P. Domokos, F. Brennecke, and T. Esslinger, Cold atoms in cavity-generated dynamical optical potentials, Rev. Mod. Phys. **85**, 553 (2013).

[7] B. Olmos, D. Yu, Y. Singh, F. Schreck, K. Bongs, and I. Lesanovsky, Long-range interacting many-body systems with alkaline-earth-metal atoms, Phys. Rev. Lett. **110**, 143602 (2013).

[8] S. Schütz and G. Morigi, Prethermalization of atoms due to photon-mediated long-range interactions, Phys. Rev. Lett. **113**, 203002 (2014).

[9] J. S. Douglas, H. Habibian, C.-L. Hung, A. V. Gorshkov, H. J. Kimble, and D. E. Chang, Quantum many-body models with cold atoms coupled to photonic crystals, Nat. Photon. **9**, 326 (2015).

[10] R. G. DeVoe and R. G. Brewer, Observation of superradiant and subradiant spontaneous emission of two trapped ions, Phys. Rev. Lett. **76**, 2049 (1996).

[11] J. Rui, D. Wei, A. Rubio-Abadal, S. Hollerith, J. Zeiher, D. M. Stamper-Kurn, C. Gross, and I. Bloch, A subradiant optical mirror formed by a single structured atomic layer, Nature (London) **583**, 369 (2020).

[12] S. Krämer, L. Ostermann, and H. Ritsch, Optimized geometries for future generation optical lattice clocks, Europhys. Lett. **114**, 14003 (2016).
[13] S. J. Masson, J. P. Covey, S. Will, and A. Asenjo-Garcia, Dicke superradiance in ordered arrays of multilevel atoms, PRX Quantum **5**, 010344 (2024).
[14] G. Facchinetti, S. D. Jenkins, and J. Ruostekoski, Storing light with subradiant correlations in arrays of atoms, Phys. Rev. Lett. **117**, 243601 (2016).
[15] H. Jen, M.-S. Chang, and Y.-C. Chen, Cooperative single-photon subradiant states, Phys. Rev. A **94**, 013803 (2016).
[16] R. J. Bettles, S. A. Gardiner, and C. S. Adams, Cooperative eigenmodes and scattering in one-dimensional atomic arrays, Phys. Rev. A **94**, 043844 (2016).
[17] I. H. Deutsch, R. J. C. Spreeuw, S. L. Rolston, and W. D. Phillips, Photonic band gaps in optical lattices, Phys. Rev. A **52**, 1394 (1995).
[18] D. V. van Coevorden, R. Sprik, A. Tip, and A. Lagendijk, Photonic band structure of atomic lattices, Phys. Rev. Lett. **77**, 2412 (1996).
[19] P. Lambropoulos, G. M. Nikolopoulos, T. R. Nielsen, and S. Bay, Fundamental quantum optics in structured reservoirs, Rep. Prog. Phys. **63**, 455 (2000).
[20] S. Rist, P. Vignolo, and G. Morigi, Photonic spectrum of bichromatic optical lattices, Phys. Rev. A **79**, 053822 (2009).
[21] S. Fernández-Vidal, S. Zippilli, and G. Morigi, Nonlinear optics with two trapped atoms, Phys. Rev. A **76**, 053829 (2007).
[22] H. Habibian, S. Zippilli, F. Illuminati, and G. Morigi, Stationary entanglement of photons and atoms in a high-finesse resonator, Phys. Rev. A **89**, 023832 (2014).
[23] R. Reimann, W. Alt, T. Kampschulte, T. Macha, L. Ratschbacher, N. Thau, S. Yoon, and D. Meschede, Cavity-modified collective Rayleigh scattering of two atoms, Phys. Rev. Lett. **114**, 023601 (2015).
[24] A. Neuzner, M. Körber, O. Morin, S. Ritter, and G. Rempe, Interference and dynamics of light from a distance-controlled atom pair in an optical cavity, Nat. Photon. **10**, 303 (2016).
[25] I. Bloch, J. Dalibard, and W. Zwerger, Many-body physics with ultracold gases, Rev. Mod. Phys. **80**, 885 (2008).
[26] H. J. Manetsch, G. Nomura, E. Bataille, X. Lv, K. H. Leung, and M. Endres, A tweezer array with 6,100 highly coherent atomic qubits, Nature (London) **647**, 60 (2025).
[27] D. Barredo, S. de Léséleuc, V. Lienhard, T. Lahaye, and A. Browaeys, An atom-by-atom assembler of defect-free arbitrary two-dimensional atomic arrays, Science **354**, 1021 (2016).
[28] M. Endres, H. Bernien, A. Keesling, H. Levine, E. R. Anschuetz, A. Krajenbrink, C. Senko, V. Vuletic, M. Greiner, and M. D. Lukin, Atom-by-atom assembly of defect-free one-dimensional cold atom arrays, Science **354**, 1024 (2016).
[29] X. Huang, W. Yuan, A. Holman, M. Kwon, S. J. Masson, R. Gutierrez-Jauregui, A. Asenjo-Garcia, S. Will, and N. Yu, Metasurface holographic optical traps for ultracold atoms, Prog. Quantum Electron. **89**, 100470 (2023).
[30] J. Zeiher, J.-y. Choi, A. Rubio-Abadal, T. Pohl, R. van Bijnen, I. Bloch, and C. Gross, Coherent many-body spin dynamics in a long-range interacting Ising chain, Phys. Rev. X **7**, 041063 (2017).
[31] A. Periwal, E. S. Cooper, P. Kunkel, J. F. Wienand, E. J. Davis, and M. Schleier-Smith, Programmable interactions and emergent geometry in an array of atom clouds, Nature (London) **600**, 630 (2021).
[32] E. Baum, A. Broman, T. Clarke, N. C. Costa, J. Mucciaccio, A. Yue, Y. Zhang, V. Norman, J. Patton, M. Radulaski, and R. T. Scalettar, Effect of emitters on quantum state transfer in coupled cavity arrays, Phys. Rev. B **105**, 195429 (2022).
[33] S. D. Jenkins, J. Ruostekoski, N. Papasimakis, S. Savo, and N. I. Zheludev, Many-body subradiant excitations in metamaterial arrays: Experiment and theory, Phys. Rev. Lett. **119**, 053901 (2017).
[34] A. Asenjo-Garcia, M. Moreno-Cardoner, A. Albrecht, H. Kimble, and D. E. Chang, Exponential improvement in photon storage fidelities using subradiance and "selective radiance" in atomic arrays, Phys. Rev. X **7**, 031024 (2017).
[35] E. Shahmoon, D. S. Wild, M. D. Lukin, and S. F. Yelin, Cooperative resonances in light scattering from two-dimensional atomic arrays, Phys. Rev. Lett. **118**, 113601 (2017).
[36] R. J. Bettles, S. A. Gardiner, and C. S. Adams, Enhanced optical cross section via collective coupling of atomic dipoles in a 2D array, Phys. Rev. Lett. **116**, 103602 (2016).
[37] J. S. Peter, S. Ostermann, and S. F. Yelin, Chirality-induced emergent spin-orbit coupling in topological atomic lattices, Phys. Rev. A **109**, 043525 (2024).
[38] J. S. Peter, S. Ostermann, and S. F. Yelin, Chirality dependent photon transport and helical superradiance, Phys. Rev. Res. **6**, 023200 (2024).
[39] J. A. Needham, I. Lesanovsky, and B. Olmos, Subradiance-protected excitation transport, New J. Phys. **21**, 073061 (2019).
[40] S. D. Jenkins and J. Ruostekoski, Controlled manipulation of light by cooperative response of atoms in an optical lattice, Phys. Rev. A **86**, 031602 (2012).
[41] M. Cech, I. Lesanovsky, and B. Olmos, Dispersionless subradiant photon storage in one-dimensional emitter chains, Phys. Rev. A **108**, L051702 (2023).
[42] I. B. Mekhov and H. Ritsch, Quantum nondemolition measurements and state preparation in quantum gases by light detection, Phys. Rev. Lett. **102**, 020403 (2009).
[43] S. Rist, C. Menotti, and G. Morigi, Light scattering by ultracold atoms in an optical lattice, Phys. Rev. A **81**, 013404 (2010).
[44] J. Perczel, J. Borregaard, D. E. Chang, H. Pichler, S. F. Yelin, P. Zoller, and M. D. Lukin, Topological quantum optics in two-dimensional atomic arrays, Phys. Rev. Lett. **119**, 023603 (2017).
[45] G. Ferioli, A. Glicenstein, L. Henriet, I. Ferrier-Barbut, and A. Browaeys, Storage and release of subradiant excitations in a dense atomic cloud, Phys. Rev. X **11**, 021031 (2021).
[46] B. Zhu, J. Cooper, J. Ye, and A. M. Rey, Light scattering from dense cold atomic media, Phys. Rev. A **94**, 023612 (2016).
[47] S. L. Bromley, B. Zhu, M. Bishof, X. Zhang, T. Bothwell, J. Schachenmayer, T. L. Nicholson, R. Kaiser, S. F. Yelin, M. D. Lukin, A. M. Rey, and J. Ye, Collective atomic scattering and motional effects in a dense coherent medium, Nat. Commun. **7**, 11039 (2016).
[48] S. Jennewein, M. Besbes, N. Schilder, S. D. Jenkins, C. Sauvan, J. Ruostekoski, J.-J. Greffet, Y. R. Sortais, and A. Browaeys, Coherent scattering of near-resonant light by a dense microscopic cold atomic cloud, Phys. Rev. Lett. **116**, 233601 (2016).
[49] D. C. Yost, A. Matveev, E. Peters, A. Beyer, T. Hänsch, and T. Udem, Quantum interference in two-photon frequency-comb spectroscopy, Phys. Rev. A **90**, 012512 (2014).

[50] T. Udem, L. Maisenbacher, A. Matveev, V. Andreev, A. Grinin, A. Beyer, N. Kolachevsky, R. Pohl, D. C. Yost, and T. W. Hänsch, Quantum interference line shifts of broad dipole-allowed transitions, Ann. Phys. **531**, 1900044 (2019).

[51] M. Horbatsch and E. Hessels, Shifts from a distant neighboring resonance, Phys. Rev. A **82**, 052519 (2010).

[52] M. Horbatsch and E. Hessels, Shifts from a distant neighboring resonance for a four-level atom, Phys. Rev. A **84**, 032508 (2011).

[53] Z. Ficek and S. Swain, *Quantum Interference and Coherence: Theory and Experiments* (Springer Science & Business Media, New York, 2005), Vol. 100.

[54] M. Kiffner, M. Macovei, J. Evers, and C. Keitel, *Vacuum-induced Processes in Multilevel Atoms* (Elsevier, Amsterdam, 2010), Chap. 3, pp. 85–197.

[55] P. Milonni, Semiclassical and quantum-electrodynamical approaches in nonrelativistic radiation theory, Phys. Rep. **25**, 1 (1976).

[56] D. A. Cardimona, M. G. Raymer, and C. R. Stroud Jr, Steady-state quantum interference in resonance fluorescence, J. Phys. B **15**, 55 (1982).

[57] D. A. Cardimona and C. R. Stroud, Spontaneous radiative coupling of atomic energy levels, Phys. Rev. A **27**, 2456 (1983).

[58] A. A. Buchheit and G. Morigi, Master equation for high-precision spectroscopy, Phys. Rev. A **94**, 042111 (2016).

[59] A. Glicenstein, G. Ferioli, N. Šibalić, L. Brossard, I. Ferrier-Barbut, and A. Browaeys, Collective shift in resonant light scattering by a one-dimensional atomic chain, Phys. Rev. Lett. **124**, 253602 (2020).

[60] G. Biagioni, B. Hofer, N. Bonvalet, D. Bloch, A. Browaeys, and I. Ferrier-Barbut, Narrowline cooling of dysprosium atoms in an optical tweezer array, Phys. Rev. A **112**, 013316 (2025).

[61] A. Konovalov and G. Morigi, Master equation for multilevel interference in a superradiant medium, Phys. Rev. A **102**, 013724 (2020).

[62] S. Jennewein, L. Brossard, Y. R. Sortais, A. Browaeys, P. Cheinet, J. Robert, and P. Pillet, Coherent scattering of near-resonant light by a dense, microscopic cloud of cold two-level atoms: Experiment versus theory, Phys. Rev. A **97**, 053816 (2018).

[63] G. Putnam, G.-D. Lin, and S. Yelin, Collective induced superradiant lineshifts, arXiv:1612.04477.

[64] R. Röhlsberger, K. Schlage, B. Sahoo, S. Couet, and R. Rüffer, Collective Lamb shift in single-photon superradiance, Science **328**, 1248 (2010).

[65] D. A. Steck, Sodium D Line Data (2000), revision 1.6 (2003), http://steck.us/alkalidata/sodiumnumbers.pdf.

[66] B. Zelener, S. Saakyan, V. Sautenkov, A. Akulshin, E. Manykin, B. Zelener, and V. Fortov, Magneto-optical trap for preparation and study of Rydberg matter, Coherent Optic. Phenom. **2**, 29 (2015).

[67] S. J. Masson, I. Ferrier-Barbut, L. A. Orozco, A. Browaeys, and A. Asenjo-Garcia, Many-body signatures of collective decay in atomic chains, Phys. Rev. Lett. **125**, 263601 (2020).

[68] N. Piovella, Cooperative decay of an ensemble of atoms in a one-dimensional chain with a single excitation, Atoms **12**, 43 (2024).

[69] G. Nienhuis and F. Schuller, Spontaneous emission and light scattering by atomic lattice models, J. Phys. B **20**, 23 (1987).

[70] J. Pellegrino, R. Bourgain, S. Jennewein, Y. R. Sortais, A. Browaeys, S. Jenkins, and J. Ruostekoski, Observation of suppression of light scattering induced by dipole-dipole interactions in a cold-atom ensemble, Phys. Rev. Lett. **113**, 133602 (2014).